

A dynamic subgrid-scale eddy viscosity model

Massimo Germano,^{a)} Ugo Piomelli,^{b)} Parviz Moin, and William H. Cabot
Center for Turbulence Research, Stanford, California 94305

(Received 14 November 1990; accepted 7 March 1991)

One major drawback of the eddy viscosity subgrid-scale stress models used in large-eddy simulations is their inability to represent correctly with a single universal constant different turbulent fields in rotating or sheared flows, near solid walls, or in transitional regimes. In the present work a new eddy viscosity model is presented which alleviates many of these drawbacks. The model coefficient is computed dynamically as the calculation progresses rather than input *a priori*. The model is based on an algebraic identity between the subgrid-scale stresses at two different filtered levels and the resolved turbulent stresses. The subgrid-scale stresses obtained using the proposed model vanish in laminar flow and at a solid boundary, and have the correct asymptotic behavior in the near-wall region of a turbulent boundary layer. The results of large-eddy simulations of transitional and turbulent channel flow that use the proposed model are in good agreement with the direct simulation data.

I. INTRODUCTION

In large-eddy simulations (LES) the effect of the large scales is directly computed, and only the small subgrid scales are modeled. Since small scales tend to be more isotropic than the large ones, it should be possible to parametrize them using simpler and more universal models than standard Reynolds stress models. Thus, most subgrid-scale (SGS) stress models are based on an eddy viscosity assumption. In the most commonly used model, developed by Smagorinsky,¹ the eddy viscosity ν_T is obtained by assuming that the small scales are in equilibrium, so that energy production and dissipation are in balance. This yields an expression of the form

$$\nu_T = (C_S \Delta)^2 |\bar{S}|, \quad (1)$$

where Δ is the filter width (which is proportional to the grid size), C_S is the Smagorinsky constant, $|\bar{S}| = (2\bar{S}_{ij}\bar{S}_{ij})^{1/2}$ is the magnitude of large-scale strain-rate tensor

$$\bar{S}_{ij} = \frac{1}{2} \left(\frac{\partial \bar{u}_i}{\partial x_j} + \frac{\partial \bar{u}_j}{\partial x_i} \right), \quad (2)$$

and \bar{u}_i is the large-scale velocity.

Lilly² determined that, for homogeneous isotropic turbulence with cutoff in the inertial subrange and Δ equal to the grid size, $C_S \approx 0.23$. In the presence of mean shear, however, this value was found to cause excessive damping of large-scale fluctuations, and in his simulation of turbulent channel flow, Deardorff³ used $C_S = 0.1$ (also with filter width equal to grid size). *A priori* tests by McMillan *et al.*⁴ on homogeneous turbulence confirmed that C_S decreases with increasing strain rate. Mason and Callen,⁵ however, found that the value $C_S = 0.2$ gave good results if the grid resolution was sufficiently fine, and concluded that values of C_S lower than 0.2 are required if the numerical resolution is insufficient. Their results, however, were not confirmed by Piomelli *et al.*,⁶ who found the optimum value of C_S to be

around 0.1 (again assuming the filter width to be equal to the grid size) even with meshes much finer than those used by Mason and Callen.⁵ It should be noted, however, that Mason and Callen⁵ did not resolve the wall layer, while Piomelli *et al.*⁶ did.

Additional modifications to the Smagorinsky model were made in the near-wall region of plane channels to force the subgrid-scale stresses to vanish at the solid boundary. Moin and Kim,⁷ for example, used damping functions to account for near-wall effects. Piomelli *et al.*⁶ chose the damping function to ensure the proper asymptotic behavior for the SGS shear stresses near the wall, but found little difference with the results obtained with the standard Van Driest damping⁸ used by Moin and Kim⁷ and others.

Yakhot *et al.*⁹ used a subgrid-scale model based on the renormalization group theory of Yakhot and Orszag¹⁰ in the large-eddy simulation of channel flow. Although the stresses predicted by the model in its original formulation go to zero at the wall without requiring any damping function, Yakhot *et al.*⁹ included an *ad hoc* factor to take into account the anisotropy of the small scales in the near-wall region. The asymptotic behavior of the stresses predicted by this model depends on the grid distribution in the wall-normal direction; for the grids commonly used, an incorrect asymptotic behavior is obtained.

Large-eddy simulations of transition to turbulence in boundary layers¹¹ and plane channel¹² show that during the early stages of transition the Smagorinsky model predicts excessive damping of the resolved structures, leading to incorrect growth rates of the initial perturbations. To overcome this difficulty an additional empiricism was introduced in the form of an intermittency function which modified the Smagorinsky constant by effectively setting it to zero during the linear and early nonlinear stages of transition.

This brief survey of the existing literature indicates that, although modifications of the Smagorinsky model have been successfully applied to the LES of transitional and turbulent flows, it is not possible to model effectively with a single, universal constant the variety of phenomena present in the

^{a)} Permanent address: Dipartimento di Ingegneria Aerospaziale, Politecnico di Torino, Turin, Italy.

^{b)} Permanent address: Department of Mechanical Engineering, University of Maryland, College Park, Maryland 20742.

flows examined. The *ad hoc* manner in which the SGS eddy viscosity has been extrapolated to the wall is far from desirable. In addition the Smagorinsky model cannot account for energy flow from small scales to large scales (backscatter), which can be significant.¹³

In this work a new, dynamic SGS stress model is proposed that attempts to overcome these deficiencies by locally calculating the eddy viscosity coefficient to reflect closely the state of the flow. This is done by sampling the smallest resolved scales and using this information to model the subgrid scales. The model presented here requires a single input parameter and exhibits the proper asymptotic behavior near solid boundaries or in laminar flow without requiring damping or intermittency functions. The model is also capable of accounting for backscatter.

In the next section, the model will be presented and its characteristics discussed. The model was tested both *a priori*, taking advantage of existing direct numerical simulation (DNS) databases, and *a posteriori* using the model in an LES calculation. The results of these tests will be discussed in Sec. III. Concluding remarks will be made in Sec. IV.

II. MATHEMATICAL FORMULATION

In large-eddy simulation, the large-scale quantities are defined by the convolution of the velocity and pressure fields with a filter function. For the purposes of this work we define two filtering operators: one is the *grid* filter \bar{G} , denoted by an overbar:

$$\bar{f}(\mathbf{x}) = \int f(\mathbf{x}') \bar{G}(\mathbf{x}, \mathbf{x}') d\mathbf{x}' \quad (3)$$

(where the integral is extended to the entire computational domain) while the other, the *test* filter \tilde{G} , is denoted by a tilde:

$$\tilde{f}(\mathbf{x}) = \int f(\mathbf{x}') \tilde{G}(\mathbf{x}, \mathbf{x}') d\mathbf{x}' \quad (4)$$

the filter width of the test filter is assumed to be larger than that of the grid filter (i.e., the test filter corresponds to a coarser mesh than the grid filter). Finally, let $\tilde{G} = \bar{G}\tilde{G}$.

By applying the grid filter to the dimensionless continuity and Navier–Stokes equations one obtains the filtered equations of motions

$$\frac{\partial \bar{u}_i}{\partial x_i} = 0, \quad (5)$$

$$\frac{\partial \bar{u}_i}{\partial t} + \frac{\partial}{\partial x_j} (\bar{u}_i \bar{u}_j) = -\frac{\partial \bar{p}}{\partial x_i} - \frac{\partial \tau_{ij}}{\partial x_j} + \frac{1}{\text{Re}} \frac{\partial^2 \bar{u}_i}{\partial x_j \partial x_j}. \quad (6)$$

In the following, x or x_1 is the streamwise direction, y or x_2 is the direction normal to the walls (which are located at $y = \pm 1$), and z or x_3 is the spanwise direction; furthermore, the distance from the nearest wall is denoted by y_w . The effects of the small scales appear in the subgrid-scale stress term

$$\tau_{ij} = \overline{u_i u_j} - \bar{u}_i \bar{u}_j, \quad (7)$$

which must be modeled.

Now apply \tilde{G} to the equations of motion: the filtered Navier–Stokes equations become

$$\frac{\partial \tilde{u}_i}{\partial t} + \frac{\partial}{\partial x_j} (\tilde{u}_i \tilde{u}_j) = -\frac{\partial \tilde{p}}{\partial x_i} - \frac{\partial T_{ij}}{\partial x_j} + \frac{1}{\text{Re}} \frac{\partial^2 \tilde{u}_i}{\partial x_j \partial x_j}, \quad (8)$$

where the subgrid-scale stress is now

$$T_{ij} = \overline{u_i u_j} - \tilde{u}_i \tilde{u}_j; \quad (9)$$

finally, consider the resolved turbulent stress \mathcal{L}_{ij} defined as

$$\mathcal{L}_{ij} = \tilde{\overline{u_i u_j}} - \tilde{u}_i \tilde{u}_j. \quad (10)$$

The resolved turbulent stresses are representative of the contribution to the Reynolds stresses by the scales whose length is intermediate between the grid filter width and the test filter width, i.e., the small resolved scales. The quantities given in (7), (9), and (10) are related by the algebraic relation¹⁴

$$\mathcal{L}_{ij} = T_{ij} - \tilde{\tau}_{ij}, \quad (11)$$

which relates the resolved turbulent stress \mathcal{L}_{ij} , which can be calculated explicitly, to the subgrid-scale stresses at the test and grid levels, T_{ij} and τ_{ij} .

The identity (11) can be exploited to derive more accurate SGS stress models by determining, for example, the value of the Smagorinsky coefficient most appropriate to the instantaneous state of the flow. Assuming that the same functional form can be used to parametrize both T_{ij} and τ_{ij} (the Smagorinsky model, for example), let M_{ij} and m_{ij} be the models for the anisotropic parts of T_{ij} and τ_{ij} :

$$\tau_{ij} - (\delta_{ij}/3)\tau_{kk} \simeq m_{ij} = -2C\bar{\Delta}^2 |\bar{S}| \bar{S}_{ij}, \quad (12)$$

$$T_{ij} - (\delta_{ij}/3)T_{kk} \simeq M_{ij} = -2\tilde{\Delta}^2 |\tilde{S}| \tilde{S}_{ij}, \quad (13)$$

where

$$\tilde{S}_{ij} = \frac{1}{2} \left(\frac{\partial \tilde{u}_i}{\partial x_j} + \frac{\partial \tilde{u}_j}{\partial x_i} \right), \quad |\tilde{S}| = \sqrt{2\tilde{S}_{mn}\tilde{S}_{mn}}, \quad (14)$$

$\bar{\Delta}$ is the characteristic filter width associated with \bar{G} , and $\tilde{\Delta}$ is the filter width associated with \tilde{G} . Substitution of (12) and (13) into (11) and contracting with \tilde{S}_{ij} gives

$$\mathcal{L}_{ij} \tilde{S}_{ij} = -2C(\bar{\Delta}^2 |\tilde{S}| \tilde{S}_{ij} \tilde{S}_{ij} - \bar{\Delta}^2 |\tilde{S}| \tilde{S}_{ij} \tilde{S}_{ij}), \quad (15)$$

from which $C(x, y, z, t)$ can be obtained in principle. The quantity in parentheses, however, can become zero, which would make C indeterminate or ill-conditioned. *A priori* tests in turbulent channel flow have shown this to be indeed the case. For the channel flow, therefore, it was assumed that C is only a function of y and t . To this end, the average of both sides of (15) is taken over a plane parallel to the wall (indicated by $\langle \rangle$) to yield

$$C(y, t) = -\frac{1}{2} \frac{\langle \mathcal{L}_{kl} \tilde{S}_{kl} \rangle}{\bar{\Delta}^2 \langle |\tilde{S}| \tilde{S}_{mn} \tilde{S}_{mn} \rangle - \bar{\Delta}^2 \langle |\tilde{S}| \tilde{S}_{pq} \tilde{S}_{pq} \rangle}; \quad (16)$$

the new dynamic eddy viscosity subgrid-scale stress model is then given by

$$m_{ij} = \frac{\langle \mathcal{L}_{kl} \tilde{S}_{kl} \rangle}{(\bar{\Delta}/\tilde{\Delta})^2 \langle |\tilde{S}| \tilde{S}_{mn} \tilde{S}_{mn} \rangle - \langle |\tilde{S}| \tilde{S}_{pq} \tilde{S}_{pq} \rangle} |\tilde{S}| \tilde{S}_{ij}. \quad (17)$$

In the present calculation, the sharp cutoff filter has been used as both test and grid filter. In finite difference calculations the test-filtered flow quantities can be computed by spatial averaging the calculated large-scale variables over a

few grid cells, for example. In more general situations, moreover, the plane average should also be replaced with appropriate local space and time averages. The model (17) implicitly assumes similarity between the SGS stresses at the grid and test levels, which are modeled using the same functional expression, namely, the Smagorinsky model.

A few remarks are in order regarding the properties and the character of the subgrid-scale stress model given by (17). First, the model gives zero SGS stress everywhere \mathcal{L}_{ij} vanishes (as long as the denominator remains finite). Such is the case in laminar flow or at solid boundaries. Furthermore, it is easy to show that in the near-wall region m_{ij} is proportional to the cube of the distance from the wall y_w , regardless of the choice of $\bar{\Delta}$ or $\tilde{\Delta}$. This is the correct asymptotic behavior for the (1,2) component of the subgrid-scale stress tensor, which, in this region, is the most significant one. To the authors' knowledge, this is the only model that satisfies this property without the use of *ad hoc* damping functions. Finally, the use of (17) implies that the modeled subgrid-scale dissipation, $\epsilon_{SGS} = m_{ij}\bar{S}_{ij}$, is proportional to the average dissipation of the resolved turbulent stresses, $\langle \mathcal{L}_{ij}\bar{S}_{ij} \rangle$, which can be either positive or negative. Thus, the model does not rule out backscatter. In the present formulation backscatter is not localized and may (or may not) occur at every point in a plane; the use of local averaging in (15), however, would allow the model to provide localized backscatter as well.

The only adjustable parameter in the model is the ratio $\tilde{\Delta}/\bar{\Delta} > 1$. The resolved turbulent stresses calculated using small values of this ratio can be contaminated by numerical errors; on the other hand, large values of it imply that the stresses due to large energy-carrying structures are used to determine the contribution of the subgrid scales. If the optimal value of $\tilde{\Delta}/\bar{\Delta}$ varies greatly from one flow to another, the applicability of the model is reduced. In the next section, large-eddy simulations of transitional and turbulent channel flow are used to address this issue.

III. RESULTS AND DISCUSSION

A priori tests of the dynamic subgrid-scale stress model (17) were carried out to determine the accuracy with which the model predicts the SGS stresses and dissipation. The tests were performed using the DNS database of Kim *et al.*¹⁵ for turbulent channel flow, and that of Zang *et al.*¹⁶ for transitional flow. Reynolds numbers are, respectively, $Re = 3300$ and 7900 (based on the centerline velocity U_c and channel half-width δ) for the turbulent case, and $Re = 8000$ for the transitional case (based on initial centerline velocity and channel half-width).

The sharp cutoff filter was applied as both grid and test filter in the streamwise and spanwise directions. No explicit test filtering was applied in the normal direction. Two commonly used definitions of the filter width were used:

$$\bar{\Delta}^3 = \bar{\Delta}_1 \bar{\Delta}_2 \bar{\Delta}_3, \quad \tilde{\Delta}^3 = \tilde{\Delta}_1 \tilde{\Delta}_2 \tilde{\Delta}_3, \quad (18)$$

and

$$\bar{\Delta}^2 = \bar{\Delta}_1^2 + \bar{\Delta}_2^2 + \bar{\Delta}_3^2, \quad \tilde{\Delta}^2 = \tilde{\Delta}_1^2 + \tilde{\Delta}_2^2 + \tilde{\Delta}_3^2, \quad (19)$$

where $\bar{\Delta}_i$ and $\tilde{\Delta}_i$ are the filter widths in each coordinate direction associated with \bar{G} and \tilde{G} , respectively; $\bar{\Delta}$ was taken

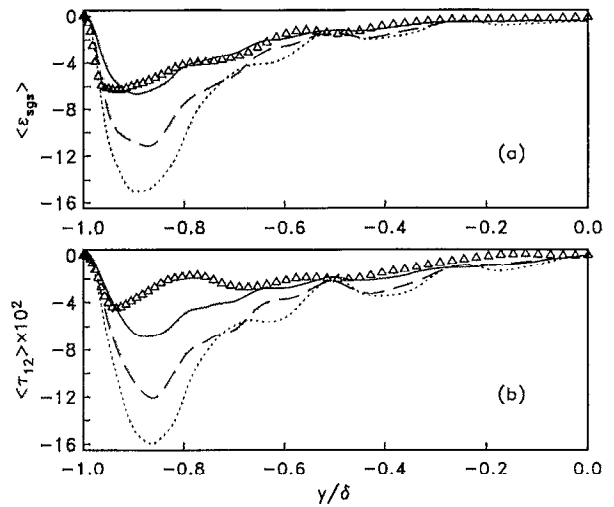


FIG. 1. Plane-averaged subgrid-scale shear stress $\langle \tau_{12} \rangle$ and dissipation $\langle \epsilon_{SGS} \rangle$; $Re = 3300$ turbulent channel flow. Δ : exact; —: $\alpha = 2$; ---: $\alpha = 3$; \cdots : $\alpha = 5$. (a) Dissipation; (b) SGS shear stress.

to be equal to twice the grid spacing, Δx_i , and various values of $\tilde{\Delta}_i$ were examined. In the following the ratio $\tilde{\Delta}_i/\bar{\Delta}_i$ will be taken equal in all directions, and denoted by α (notice, however, that no explicit filtering is applied in the wall-normal direction).

The mean subgrid-scale shear stress $\langle \tau_{12} \rangle$ and dissipation $\langle \epsilon_{SGS} \rangle$ are compared with the modeled ones in Fig. 1 for various filter widths in the turbulent channel flow. Equation (19) was used to define the filter width. The choice $\alpha = 2$ was found to yield the best results. However, actual large-eddy simulations with the dynamic model appear to be very insensitive to α (see below). With this choice $\bar{\Delta}$ corresponds to a wave number in the decaying region of the one-dimensional energy spectrum, while $\tilde{\Delta}$ represents a wave number in the flat region. In Fig. 2, the product $C\bar{\Delta}^2$ is plotted as function of the wall coordinate $y^+ = u_\tau y_w/\nu$ [where $u_\tau = (\tau_w/\rho)^{1/2}$ is the friction velocity, τ_w is the wall shear, and ρ is the fluid density]; the expected y^+ behavior is evident. At the channel center $C \approx 0.023$ when (18) is used; the square root of this value is 0.15, about 50% larger than the value of C_S used by Deardorff.³ When (19) is used, at the channel center $C \approx 7 \times 10^{-4}$, which gives a value of 0.026 for

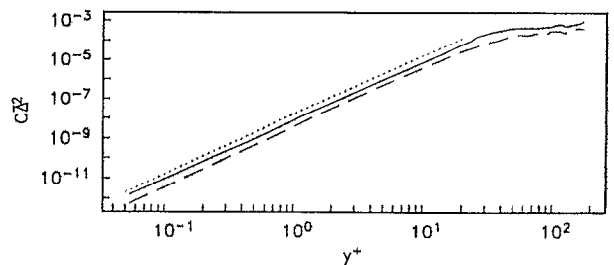


FIG. 2. Variation of $C\bar{\Delta}^2$ [defined in Eq. (17)] with distance from the wall; $Re = 3300$ turbulent channel flow. $\alpha = 2$. —: $C\bar{\Delta}^2$ obtained using (18); ---: $C\bar{\Delta}^2$ obtained using (19); \cdots : $C\bar{\Delta}^2 \sim y^+$.

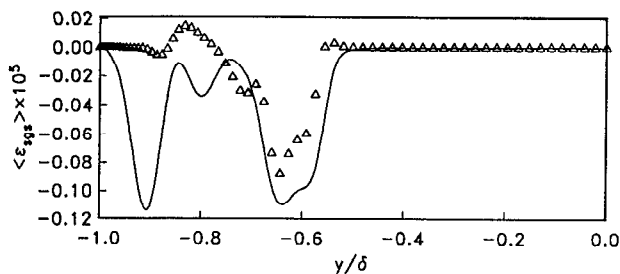


FIG. 3. Plane-averaged subgrid-scale dissipation $\langle \epsilon_{SGS} \rangle$; transitional flow, $t = 176$. Δ : exact; —: $\alpha = 2$.

the Smagorinsky constant. The issue of the sensitivity of the numerical results to the choice of filter width and of α will be addressed later. The model was also tested in transitional flow for $\alpha = 2$ (Fig. 3). The SGS dissipation predicted by the Smagorinsky model for this case is many orders of magnitude larger, and peaks much closer to the wall than the exact one.¹¹

To further determine the accuracy of the dynamic SGS model (17), it was also tested *a posteriori* in the LES of transitional and fully developed turbulent channel flow. Initial conditions consisted of the parabolic mean flow, on which a 2-D Tollmien-Schlichting (TS) mode of 2% amplitude and a 3-D TS mode of 0.02% amplitude were superimposed. The initial conditions and Reynolds number matched those of the direct simulation of Ref. 16. The governing equations (5) and (6) were integrated in time using a pseudospectral Fourier-Chebyshev collocation method.¹⁷ Both filter widths (18) and (19) were used; the final results were insensitive to this choice, so only those obtained using Eq. (18) will be presented. The ratio $\alpha = 2$ was chosen. At the initial stages $8 \times 49 \times 8$ grid points were used; the mesh was then progressively refined up to $48 \times 65 \times 64$ points; the dimensions of the computational domain were $2\pi\delta$ in the streamwise direction and $4\pi\delta/3$ in the spanwise direction. Periodic boundary conditions were applied in the streamwise and spanwise directions; no-slip conditions were applied at the walls.

The time development of the mean wall shear stress $\langle \tau_w \rangle$ is compared in Fig. 4 with the DNS results of Ref. 16 and with the results of the LES of Ref. 12, which used a Smagorinsky model including Van Driest damping and an

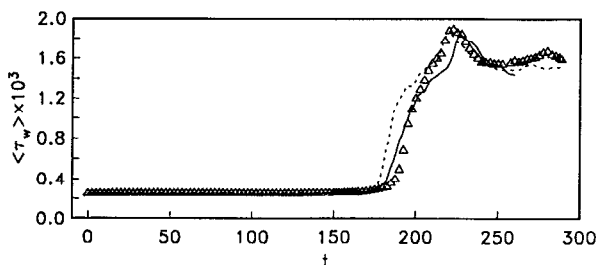


FIG. 4. Time development of the plane-averaged wall shear stress $\langle \tau_w \rangle$ in $Re = 8000$ transitional channel flow. Δ : DNS;¹⁶ —: present results; \cdots : LES.¹²

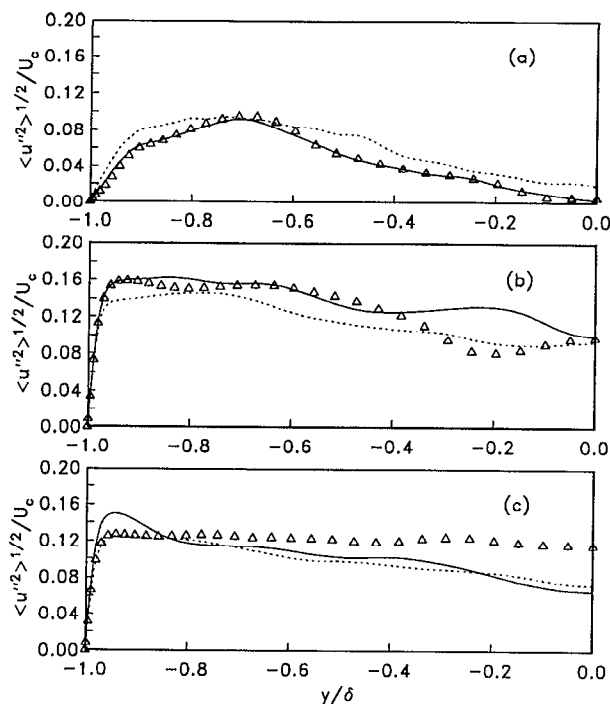


FIG. 5. Plane-averaged rms turbulence intensities $\langle u''^2 \rangle^{1/2}$ in $Re = 8000$ transitional channel flow. Δ : Filtered DNS;¹⁶ —: present calculation; \cdots : LES.¹² (a) $t = 176$; (b) $t = 200$; (c) $t = 220$.

ad hoc intermittency function; the present results compare very well with the finely resolved DNS. A coarse direct simulation which can adequately resolve the early stages of transition (up to $t \approx 170$) cannot predict the drag crisis (Fig. 4) and the breakdown process.¹² With the present model, on the other hand, the predicted peak wall stress is within 3% of the DNS result. The root-mean-square fluctuation of $\langle u''^2 \rangle^{1/2}$ (where $u_i'' = \bar{u}_i - U_i$ and $U_i = \langle \bar{u}_i \rangle$) and the Reynolds shear stress $\langle u''v'' \rangle$, shown in Figs. 5 and 6, are in fair agreement with the DNS results. The DNS results have been filtered using the same filter employed in the LES calculation. Discrepancies between the LES and DNS results at late stages of transition may be due to the fact that, at these times, slight differences in the prediction of the onset of transition may result in significant differences in the instantaneous fields. The capability of the model to predict average backscatter is evidenced by the fact that for $t \leq 185$ the eddy viscosity was negative for significant regions of the channel.

Once fully developed turbulent flow was achieved, statistics were accumulated. The Reynolds number of the turbulent flow was $Re = 6100$ based on centerline velocity and channel half-width. The mean velocity profile is shown in Fig. 7, normalized by the friction velocity u_τ , and by the bulk velocity U_b ,

$$U_b = \frac{1}{2\delta} \int_{-\delta}^{\delta} \langle \bar{u} \rangle dy. \quad (20)$$

An inadequate resolution of the wall layer results in a low value of wall stress that is reflected in a high value of the intercept of the logarithmic layer in Fig. 7(b). The overall agreement of the LES results with the DNS data is fairly

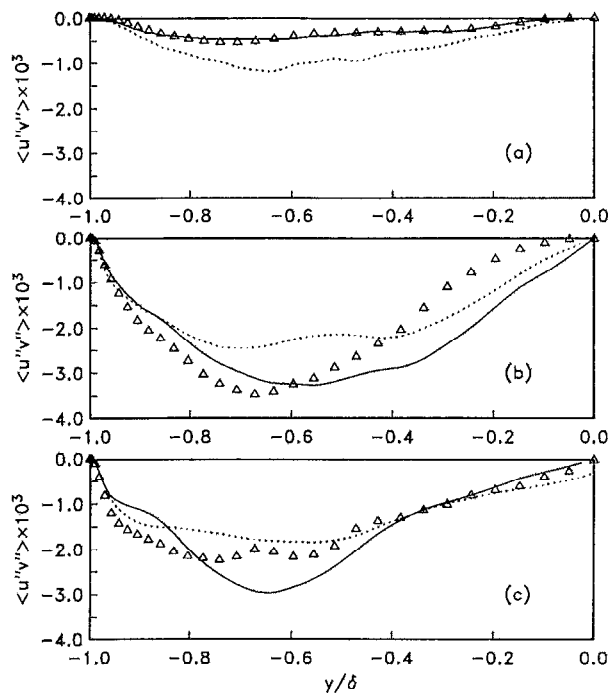


FIG. 6. Plane-averaged Reynolds stress $\langle u''v'' \rangle$ in $Re = 8000$ transitional channel flow. Δ : Filtered DNS;¹⁶ —: present calculation; \cdots : LES.¹² (a) $t = 176$; (b) $t = 200$; (c) $t = 220$.

good. The turbulence intensities $\langle u_i''^2 \rangle^{1/2}$ normalized by the friction velocity u_τ are shown in Fig. 8. The DNS results have been filtered using the same filter employed in the LES calculation. In general, the dynamic model gives more accurate results than the Smagorinsky model used by Piomelli and Zang.¹² The peak of the streamwise turbulent kinetic energy occurs near $y^+ = 12$, a value also obtained by experi-

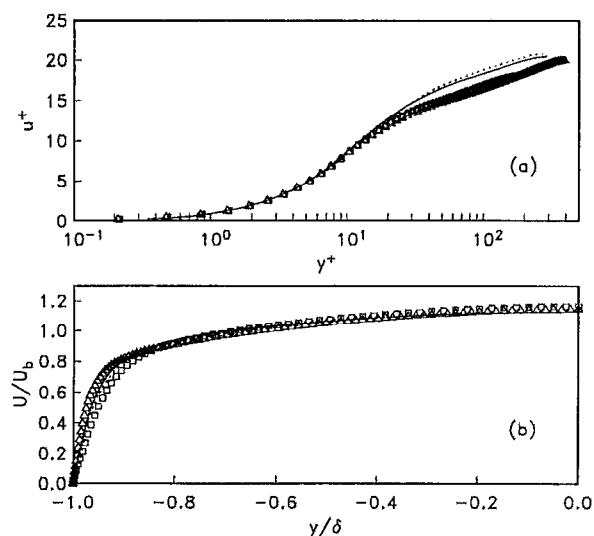


FIG. 7. Mean velocity profile in fully developed turbulent channel flow. Δ : $Re = 7900$ filtered DNS;¹⁵ \square : $Re = 3300$ filtered DNS;¹⁵ —: present calculation; \cdots : LES.¹² (a) Wall coordinates; (b) global coordinates.

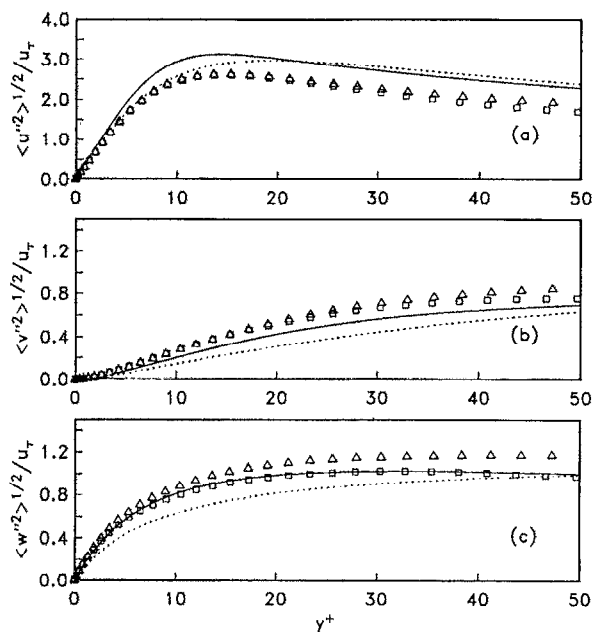


FIG. 8. Turbulence intensities $\langle u_i''^2 \rangle^{1/2}$ in fully developed turbulent channel flow. Δ : $Re = 7900$ filtered DNS;¹⁵ \square : $Re = 3300$ filtered DNS;¹⁵ —: present calculation; \cdots : LES.¹² (a) u ; (b) v ; (c) w .

ments and numerical simulations; the mean streak spacing was found to be $\lambda^+ = 140$, somewhat larger than the established value of 100, which is also expected of large-eddy simulations. The skewness and flatness factors of the three velocity components are shown in Fig. 9. They compare fairly well with the DNS results. Note that in contrast to turbulence intensities, higher-order statistics from LES are compared with unfiltered DNS results.

To investigate the effect of the parameter α on the numerical results we performed a calculation in which the val-

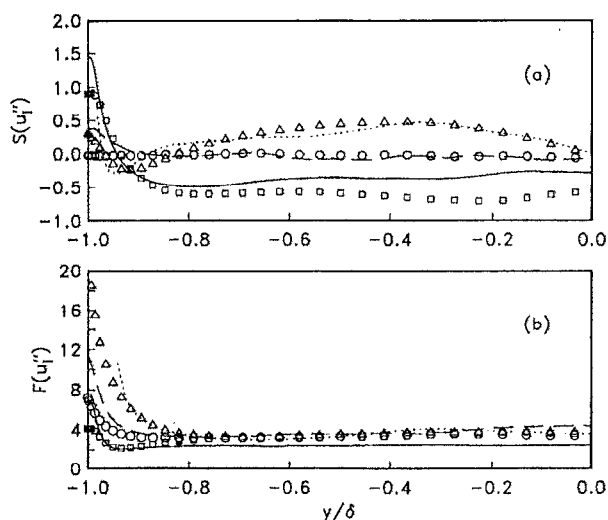


FIG. 9. Skewness and flatness factors of u , in fully developed turbulent channel flow. —: u'' ; \cdots : v'' ; $---$: w'' from the present calculation. \square : u'' ; Δ : v'' ; \circ : w'' from $Re = 3300$ DNS.¹⁵ (a) Skewness; (b) flatness.

ue $\alpha = 4$ was used. This amounts to changing the coefficient of the first term in the denominator of Eq. (17) by almost a factor of 4. The results were found to be very insensitive to this parameter: differences in the mean and rms velocities were less than 3%; the wall stresses differed by less than 6%. The maximum resolved shear stress was larger by approximately 4% in the calculation with $\alpha = 2$, and the subgrid scale contribution smaller by the same amount. The insensitivity of the large-eddy simulation results to the value of α is contrary to one's expectations from the *a priori* tests (Figs. 1 and 3) and casts some doubt on the utility of *a priori* tests in providing quantitative data for LES.

IV. CONCLUDING REMARKS

A new eddy viscosity subgrid-scale stress model has been presented in which the smallest resolved scales are dynamically tested to predict the behavior of the subgrid scales. This model is based on the algebraic identity (11) between the resolved turbulent stresses and the subgrid-scale stresses obtained using two filters, the grid filter and the test filter. The model coefficient is obtained dynamically as the calculations progress. This procedure exploits the spectral information on the energy content of the smallest resolved scales provided by LES calculations to dynamically adjust the model. The only input to the model is the ratio of test filter width to grid filter width, α . Among the useful properties of the model is its proper asymptotic behavior near the wall without the use of *ad hoc* damping functions.

Large-eddy simulations of transitional and fully developed turbulent channel flow were also carried out. The results were in good agreement with those of direct simulations, and better than those of LES that used the Smagorinsky model with *ad hoc* damping and intermittency functions. Doubling the value of α did not affect the numerical results significantly.

Investigation of the properties of this model when the

box filter is employed is desirable. The sensitivity of the results to the choice of α should also be further investigated in flow configurations much different from those studied here. Finally, the use of local space and time averages instead of the plane average used to obtain (17) should be attempted.

ACKNOWLEDGMENT

Partial support for the second author (UP) was provided by the Office of Naval Research under Grant No. N00014-89-J-1531.

- ¹J. Smagorinsky, Mon. Weather Rev. **91**, 99 (1963).
- ²D. K. Lilly, NCAR Manuscript 123, 1966.
- ³J. W. Deardorff, J. Fluid Mech. **41**, 453 (1970).
- ⁴O. J. McMillan, J. H. Ferziger, and R. S. Rogallo, AIAA Paper No. 80-1339, 1980.
- ⁵P. J. Mason and N. S. Callen, J. Fluid Mech. **162**, 439 (1986).
- ⁶U. Piomelli, P. Moin, and J. H. Ferziger, Phys. Fluids **31**, 1884 (1988).
- ⁷P. Moin and J. Kim, J. Fluid Mech. **118**, 341 (1982).
- ⁸E. R. Van Driest, J. Aeronaut. Sci. **23**, 1007 (1956).
- ⁹A. Yakhot, S. A. Orszag, V. Yakhot, and M. Israeli, J. Sci. Comput. **4**, 139 (1989).
- ¹⁰V. Yakhot and S. A. Orszag, J. Sci. Comput. **1**, 3 (1986).
- ¹¹U. Piomelli, T. A. Zang, C. G. Speziale, and M. Y. Hussaini, Phys. Fluids A **2**, 257 (1990).
- ¹²U. Piomelli and T. A. Zang, Comput. Phys. Commun. **65**, 224 (1991).
- ¹³U. Piomelli, W. H. Cabot, P. Moin, and S. Lee, Phys. Fluids A **3**, 1766 (1991).
- ¹⁴M. Germano, CTR Manuscript 116, 1990.
- ¹⁵J. Kim, P. Moin, and R. D. Moser, J. Fluid Mech. **177**, 133 (1987). The high Reynolds number DNS was performed after the publication of Ref. 11; the same numerical method used for the lower Reynolds number case was employed, and $256 \times 193 \times 192$ grid points were used to give the same resolution, in wall units, of the lower Reynolds number case.
- ¹⁶T. A. Zang, N. Gilbert, and L. Kleiser, in *Instability and Transition*, edited by M. Y. Hussaini and R. G. Voigt (Springer-Verlag, New York, 1990), pp. 283–299.
- ¹⁷T. A. Zang and M. Y. Hussaini, in *Nonlinear Wave Interactions in Fluids*, edited by R. W. Miksad, T. R. Akylas, and T. Herbert (ASME, New York, 1987), pp. 131–145.